A&A 485, 735–742 (2008)
DOI: 10.1051/0004-6361:20066618

Astronomy & Astrophysics

Modeling the interstellar aromatic infrared bands with co-added spectra of PAHs

Amit Pathak⋆ and Shantanu Rastogi

Physics Department, DDU Gorakhpur University, Gorakhpur 273009, India
e-mail: shantanu_r@hotmail.com

Received 22 October 2006 / Accepted 21 March 2008

ABSTRACT

Aims. The observed variations in profiles of the interstellar aromatic infrared bands correlate with the object type and are indicative of PAH populations existing in different sources. Spectroscopic studies of PAHs can provide tools for interpreting the variations accompanying the AIBs. As the observed spectra results from a mix of possible species in the region, we try to model this composite spectra by co-adding emissions from PAHs in different size groups.
Methods. Theoretical IR data of PAHs having 10 to 96 carbon atoms is used to obtain emission spectra. The models are taken in size groups made up of small, medium, and large PAHs.
Results. The models show a good profile match with observations for the 7.7 μm complex having sub-features at 7.6 and 7.8 μm. The 7.6 μm sub-feature dominates in the spectra of medium-sized PAH cations, matching observations from UV-rich interstellar environments. The 7.8 μm component is more intense in the spectra of large PAH cations (model III), correlating with observations from benign astrophysical regions. A possible interpretation of the observations of C−H out-of-plane bend modes and the weak outliers on the blue side of the intense 11.2 μm band is proposed. The models provide pointers to possible PAH populations in different regions.

Key words. molecular data – ISM: molecules – infrared: general – infrared: ISM

1. Introduction

The mid-infrared emission bands at 3.3, 6.2, 7.7, 8.6, 11.2, and 12.7 μm (3030, 1610, 1300, 1160, 890, and 790 cm^{-1}) and beyond (Gillett et al. 1973; Cohen et al. 1989; Geballe et al. 1989; ISO results 1996; Peeters et al. 2002, 2004a) observed in diverse astrophysical sources are popularly known as aromatic infrared bands (AIBs). These bands have been attributed to emission from the isolated gas phase PAH molecules present in the interstellar medium (ISM) (Léger & Puget 1984; Allamandola et al. 1985; Puget & Léger 1989; Allamandola et al. 1989). The ubiquity of AIBs make PAHs an important interstellar family of molecules having significant carbon reserves. The emission process of a PAH molecule involves the absorption of an energetic photon ranging from near UV to near IR (Allamandola et al. 1989; Li & Draine 2002; Smith et al. 2004; Mattioda et al. 2005a,b), which renders it into a vibrationally excited state through internal vibrational redistribution (Allamandola et al. 1989; Puget & Léger 1989). The PAH molecules de-excite mainly through IR fluorescence with the emission bands corresponding to fundamental modes of vibrations set up within the molecule. PAHs may also relax via visible phosphorescence and/or fluorescence and are proposed as carriers of the extended red emission (ERE) (Witt et al. 2006) and the blue luminescence (BL) (Vijh et al. 2005).

Extrapolating the spacing between 6.2 and 7.7 μm PAH bands produced from experimental data, Hudgins & Allamandola (1999b) conclude that PAHs with 50–80 carbon atoms dominate the mid-IR emission. Studies testing the photo-physical stability of PAHs (Schutte et al. 1993; Allain et al. 1996a,b; LePage et al. 2003) have reached a similar conclusion. Devoted experimental (Szczepanski & Vala 1993; Hudgins et al. 1994; Hudgins & Allamandola 1995; Hudgins & Sandford 1998; Cook et al. 1996; Kim et al. 2001; Kim & Saykally 2002) and theoretical research (Langhoff 1996; Bauschlicher & Bakes 2000; Bauschlicher 2002; Pathak 2006; Pathak & Rastogi 2005, 2006, 2007) has resulted in considerable IR information of a large number of PAHs of varying sizes and ionized states. These results serve as input in theoretical emission models (Bakes et al. 2001a,b; Pech et al. 2002; Joblin et al. 2002; Mulas et al. 2003, 2006a,b) for direct comparison with observations. Such modeling studies emphasize the contribution of PAH cations towards AIBs along with neutral PAHs contributing to a lesser extent. The fractional abundance of cations and neutrals depends on the astrophysical environment where the AIBs are being observed. Current understanding points towards the dominance of cations in harsh UV-rich conditions of reflection nebulae and HII regions, while a mixture of neutrals and cations in relatively cool environments of late-type carbon-rich stars (Allamandola et al. 1999).

Over the years, developments in observational accuracy using space telescopes have improved the quality of data and a large and diverse sample of astrophysical sources have been examined that exhibit these mid-IR bands (Peeters et al. 2002, 2004a; Van Diedenhoven et al. 2004). Observations from ISO (1996) and SPITZER (2004) have provided good quality data that has revealed significant variations and finer profile details of the individual AIBs. Of strong interest is the peak position of the 6.2 μm band, the broad composite 7.7 μm band (Peeters et al. 2002), variations accompanying the asymmetric 11.2 μm band,

⋆ *Current address*: Inorganic and Physical Chemistry Department, I.I.Sc., Bangalore, India.

features at 12.7, 13.3 μm, and at higher wavelengths (Hudgins & Allamandola 1999a; Hony et al. 2001). Few new features detected around 6.7, 10.1, 15.8, 17.4, and 19.0 μm have added to the AIB numbers (Werner et al. 2004; Peeters et al. 2004b). These revelations make studies of different PAH groups important for gaining a better understanding of AIBs.

In this report we attempt to model the variations associated with AIBs using our existing IR database of PAHs (Pathak 2006; Pathak & Rastogi 2005, 2006, 2007). The IR data consisting of PAHs with 10 to 96 carbon atoms is computed using the GAMESS ab-initio program (Schmidt et al. 1993) under DFT using B3LYP functionals in conjunction with 4-31G basis expansion. To model the observed profile variations in AIBs, first the thermal emission model (Schutte et al. 1993; Pech et al. 2002) is used to obtain the emission spectra of each PAH. Then for PAHs in different size groups the emission spectra is co-added to model AIB spectra. The comparisons with observations give insight into possible PAH size distribution and their processing in different astrophysical regions. Attempt is made to put constraints on the PAH population residing in different interstellar environments.

2. Emission model

Emission spectra of PAHs are needed for a meaningful comparison with observations (Schutte et al. 1993; Cook & Saykally 1998; Pech et al. 2002; Mulas et al. 2003). Léger et al. (1989) and Schutte et al. (1993) have shown that cooling a PAH via transitions in an emission cascade can be described by the thermal approximation if the average energy of the mode under consideration is smaller than the total energy of the excited PAH. The thermal model is known to break down for emission in low-energy modes near the end of the emission cascades (Joblin et al. 2002; Mulas et al. 2006a,b). In the present work a strong background radiation field, corresponding to blackbody temperature $T = 40\,000$ K, is considered. This ensures that the total internal energy of excited PAH is much higher than the energy of any emission mode and thermal approximation holds. A similar approach is taken by Cook & Saykally (1998) and Pech et al. (2002).

We compute the emission spectrum for each individual PAH with calculated absorption spectrum used as input. As in Schutte et al. (1993), the PAHs are considered in a exciting radiation field similar to what surrounds Θ^1 Ori C, corresponding to blackbody temperature $T_* = 40\,000$ K. The PAH molecules absorb photons of all energies with a cut off at 13.6 eV giving rate of photon absorption as

$$R_{\rm abs} = \int_0^{13.6} \frac{B_\nu \sigma_\nu}{h\nu} {\rm d}\nu \tag{1}$$

where B_ν is the Planck function, σ_ν the photo-absorption cross-section, and ν the absorbed UV radiation frequencies. For each PAH, σ_ν are taken from http://astrochemistry.ca.astro.it/database/ (Malloci et al. 2007). The differences in the shape of the photo-absorption is apparent mostly in the low-energy part of the spectrum, which for the UV-rich spectrum in the present emission models is irrelevant. For PAHs with no entry in the database, a scaled photo-absorption cross-section of PAHs closest in size (number of carbon atoms) is used. The scaling is approximated by a factor $N_{\rm C2}/N_{\rm C1}$ (Mulas et al. 2006b), with PAH having $N_{\rm C1}$ carbon atoms as the proxy for the larger molecule with $N_{\rm C2}$ carbon atoms.

The absorption of a high-energy photon of frequency ν excites the PAH molecule to an internal energy equivalent to peak temperature $T_{\rm p}$ that depends on the heat capacity of the PAH. In the harmonic approximation, this $T_{\rm p}$ is obtained from

$$U(T) = \sum_{i=1}^{m} \frac{hc\,\omega_i}{\exp(hc\,\omega_i/kT) - 1} \tag{2}$$

where i corresponds to vibrational modes within individual PAHs having frequency ω_i in cm^{-1}, and m is the total number of vibrational modes ($3N - 6$; N being the number of atoms).

To ensure the validity of the thermal approximation fall in peak temperature for each PAH is calculated assuming integrated emission of highest frequency modes corresponding to the C−H stretch vibrations. For naphthalene, the smallest PAH in the sample, peak temperature falls by 11.3%, which is the maximum. While for $C_{96}H_{24}$, the largest PAH, the fall in peak temperature is less than 0.5%. This is small enough to justify the use of a thermal model in the exciting radiation field considered.

The molecule cools down from the peak temperature $T_{\rm p}$ through its different vibrational modes with cascade transitions from levels $v \rightarrow v - 1$. The emission photon flux ϕ_i of the ith mode is given as

$$\phi_i = A_i^{1,0} \times [\exp(hc\,\omega_i/kT) - 1]^{-1} \tag{3}$$

where the Einstein coefficients $A_i^{1,0}$ are obtained from the absorption intensities S_i (in units of Km/mol) (Cook & Saykally 1998) by the relation

$$A_i^{1,0} = (1.2512 \times 10^{-7})\,\omega_i^2\,S_i. \tag{4}$$

For a fall in internal energy by ΔU, the fractional energy emitted in the ith mode is then given as

$$\Delta E_i(T) = \frac{\phi_i \times \omega_i}{\sum_{i=1}^{m} \phi_i \times \omega_i} \times \Delta U(T). \tag{5}$$

The fractional energy E_i is integrated over the cooling range from $T_{\rm p}$ to a temperature of 50 K below which the energy emitted is negligible. The value of ΔU corresponding to a fall in temperature by 1 K is taken at each T. This emitted energy is weighted by the rate of photon absorption (Eq. (1)) and integrated over the whole distribution of absorbed photons.

The emission spectra thus obtained for each PAH is then used to model composite spectra from groups of PAHs. Spectra of PAHs in each group are co-added assuming an equal number of each species in the ISM.

3. Spectral models and their astrophysical significance

The AIBs result from composite emission of a number of PAHs; consequently, profile variations associated with AIBs in different sources reflect the presence of different PAH groups therein. Factors like anharmonicity and rotational broadening also affect line widths and shape (Pech et al. 2002). Anharmonicity induces small asymmetry in the profile, and the rotational widths too are small and get smaller for larger PAHs. The contribution of these effects is <5 cm^{-1} (Mulas et al. 2006a; Pech et al. 2002), while a typical peak width under interstellar conditions is ~30 cm^{-1} (Allamandola et al. 1989). Experimental measurements on a few individual PAHs show a near linear dependence on band width and temperature with intrinsic widths between 10–20 cm^{-1} around 1000 K (Joblin et al. 1995; Pech et al. 2002). In obtaining the composite emission spectra, we neglect anharmonicity and rotational broadening and assume a Lorentzian

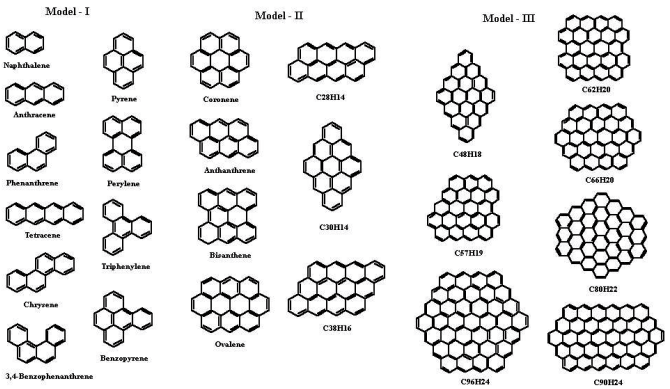

Fig. 1. PAHs constituting the three models.

profile with an *FWHM* of 20 cm^{-1}. Several modes closer than this may collocate and result in a single broad peak. Three distinct models are presented to understand the gross changes (intensity, as well as profile variations) in the PAH spectra with different PAH size groups. Individual PAHs used in the models are displayed in Fig. 1.

Model I comprises co-added emission spectra of small PAHs (≤20 carbon atoms) consisting of naphthalene, anthracene, phenanthrene, pyrene, tetracene, chrysene, 3, 4-benzophenanthrene, triphenylene, perylene, and benzopyrene. Model II (PAHs with 20 to 40 carbon atoms) is derived from a mixture of anthanthrene, coronene, bisanthene, ovalene, $C_{28}H_{14}$, $C_{30}H_{14}$, and $C_{38}H_{16}$. Model III uses the co-added spectra of large PAHs (>40 carbon atoms), which includes $C_{48}H_{18}$, $C_{57}H_{19}$, $C_{62}H_{20}$, $C_{66}H_{20}$, $C_{80}H_{22}$, $C_{90}H_{24}$, and $C_{96}H_{24}$. All the three models consider equal number of constituent PAHs. Emission spectra of the three models as neutral and cation are compared in Figs. 2 and 3. In the composite spectra, each peak may result from the overlap of different modes in different PAHs. Therefore only a general assignment of intensity peaks with vibrational modes is possible.

The spectra of neutrals (Fig. 2) is dominated by the C−H stretch and C−H out-of-plane bend vibrations. Comparison of the absorption calculations with experimental data wherever available shows that the C−H stretch intensity is overestimated by about 1.4 to 2.0 times (Pathak & Rastogi 2007). Use of larger basis sets, i.e., 6-31G or 6-31G**, in place of 4-31G, provide better representation of the orbitals and consequently a good C−H stretch intensity match with experiments. Use of larger basis for some of the PAHs incorporated in model I shows that computational effort increases greatly and the scaling procedure also gets complicated, but there is a negligible change in intensity or in the position of modes other than C−H stretch (Pathak & Rastogi 2007). Therefore, for the study of profiles and relative intensity of all other modes, the 4-31G basis is suitable, while giving qualitative information on the C−H stretch.

In the cascade emission model, low temperatures contribute little towards the intensity of modes at higher frequencies. The contribution is diminished further in the case of large PAHs that are excited to lower peak temperatures. In the large PAH model III, the intensity of the C−H stretch mode is small compared to the models with smaller PAHs. The observed C−H stretch (3.3 μm) and C−H out-of-plane bend (11.2 μm) intensity ratio is a suitable parameter constraining the size distribution of PAHs (Schutte et al. 1993; Pech et al. 2002).

The absorption intensity of C−H stretch vibrations reduce drastically upon ionization, while small intensity variations are

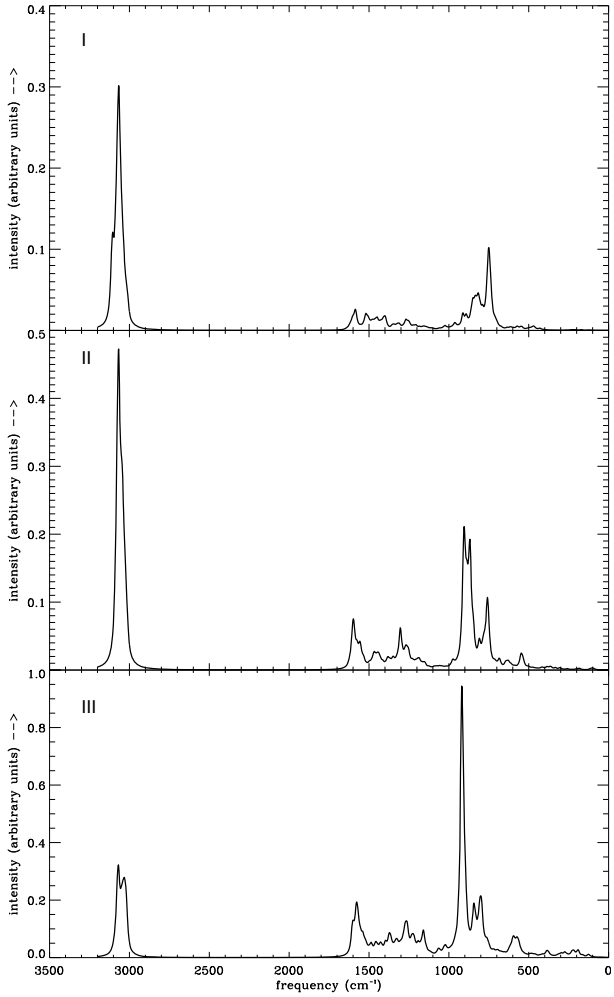

Fig. 2. Model spectra of co-added emissions from neutral PAHs with (I) less than 20 C atoms, (II) 20 to 40 C atoms, (III) more than 40 C atoms.

observed for the C−H wag modes. The intensity of the C−H stretch mode depends on the charge density near the hydrogen atoms (Hudgins et al. 2001; Pathak & Rastogi 2005, 2006). In cations this (positive) charge density increases, consequently the C−H stretch intensity gets drastically reduced. In larger PAH cations due to the distribution of the acquired positive charge over more atoms, the absorption in C−H stretch mode is significant (Pathak & Rastogi 2006, 2007). This and the temperature effect in the cascade emission model is reflected in the composite emission spectra (Fig. 3) showing significant C−H intensity in model II and reduced intensity in models I and III.

3.1. C–C stretch modes

Among the AIBs, the 6.2 and 7.7 μm emission features are the most intense. The C−C stretch vibrations set up in ionized PAH molecules give rise to these bands. The 6.2 μm band has some contributions from C−H in plane bend modes as well (Pathak & Rastogi 2005). Profile variations observed in these bands are a direct measure of the background environments that excite the PAHs.

Peeters et al. (2002) report detailed ISO observations of 57 diverse sources in the 6 to 9 μm range and, based on intricate position and profile variations, classify these bands into three classes *A*, *B*, and *C*. Class *A* has the 6.2 μm band maximum

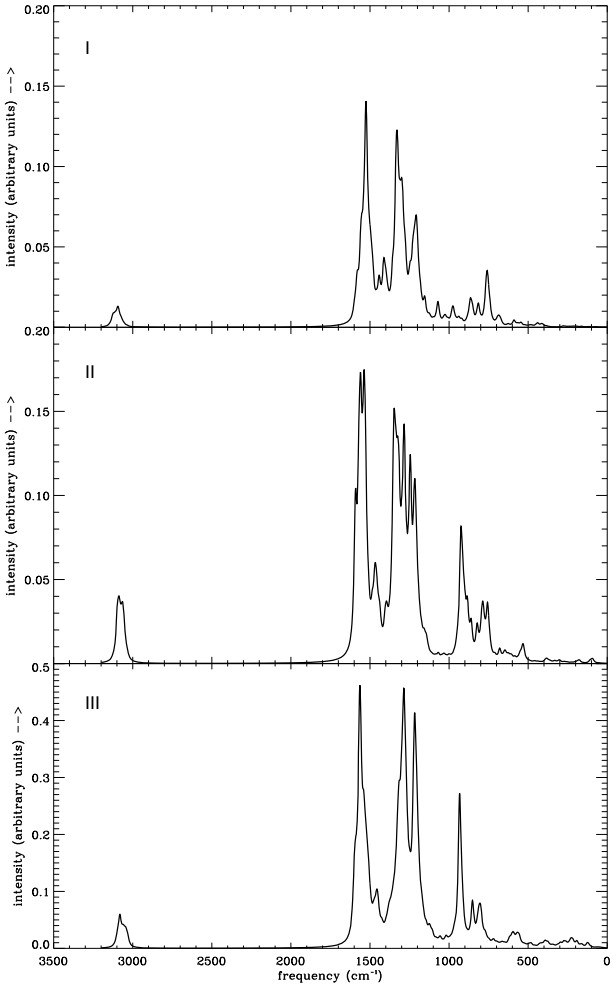

Fig. 3. Model spectra of co-added emissions from PAH cations with (I) less than 20 C atoms, (II) 20 to 40 C atoms, (III) more than 40 C atoms.

in between 6.20 and 6.23 μm and the 7.7 μm complex peak at 7.6 μm. Bands between 6.23 and 6.29 μm and a peak at 7.8 μm are classified as class *B*. Bands centered at 6.29 and redder are classified as class *C*. Out of the 57 sources reported, 42 belong to class *A*, 12 to class *B*, and 2 sources are classified as *C*. Similar profiles have also been reported by other observations for reflection nebulae and Herbig Ae/Be stars (Bregman & Temi 2005; Sloan et al. 2005).

All three PAH cation models (Fig. 3) show intense broad peaks corresponding to 7.7 and 6.2 μm modes. The peaks are at 1330 (7.52 μm) and 1526 cm^{-1} (6.55 μm), at 1347 (7.42 μm) and 1537 cm^{-1} (6.50 μm), and at 1285 (7.78 μm) and 1564 cm^{-1} (6.39 μm) respectively for models I, II, and III. The C–H in-plane vibrations have peaks around 1215 cm^{-1} (8.23 μm) in all the models with little variation in the peak position.

Observations show that the 7.7 μm AIB incorporates two sub-components at 7.6 μm (1315 cm^{-1}) and at 7.8 μm (1282 cm^{-1}) (Cohen et al. 1989; Bregman et al. 1989; Peeters et al. 2002). The 7.6 μm feature tends to dominate the emission spectra of regions involved in processing PAHs and other molecules i.e., star-forming regions, HII regions, and reflection nebulae, etc. The 7.8 μm component dominates in environments where the PAHs are relatively fresh and unprocessed, such as planetary nebulae and objects evolving from the asymptotic giant branch (AGB) phase of stellar evolution. Similar

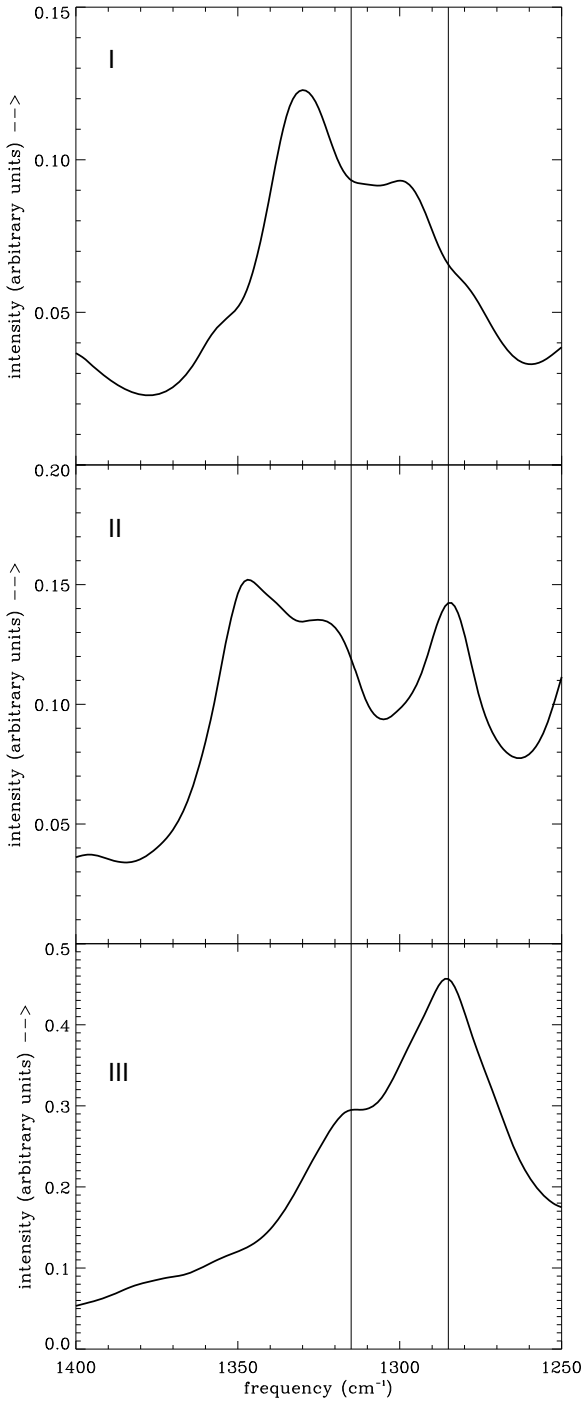

Fig. 4. Emission spectra of three cation models in the 1250 to 1400 cm^{-1} region. The observed 7.7 μm AIB lies within the two parallel lines.

sub-components for the 7.7 μm band are obtained in the present models. This provides useful insight into the PAH size and charge state in different interstellar environments.

Figure 4 shows the expanded spectra in the 1250–1400 cm^{-1} region for the cation models of Fig. 3. The two parallel lines at 1285 and 1315 cm^{-1} enclose the observed 7.7 μm complex. Two sub-features that constitute the 7.7 μm band having a separation of 30–40 cm^{-1} are evident in the three models. Model I has a dominant feature at 1330 cm^{-1} (7.52 μm) corresponding to the observed 7.6 μm component along with a shoulder at

Table 1. Band position and strength ratios of the two components of 7.7 μm composite.

Model	7.6	7.8	Diff (cm^{-1})[1]	$Diff^{2}_{obs}$ (cm^{-1})	$I_{7.6}/I_{7.8}$[1]	Obs $I_{7.6}/I_{7.8}$[2]
Model I	1330	1300	30		1.32	
Model II	1347	1285	62	~30	1.06	1.56 (NGC 2023)
						1.35 (Orion peak 2)
						1.20 (IRAS 23133)
Model III	1315	1285	30	~45	0.65	0.64 (NGC 7027)
						0.52 (IRAS 17047)
						0.42 (HD 44179)

[1] Difference in the band position and intensity ratio of the two components of the 7.7 μm composite as calculated from the theoretical spectral models; [2] The observed results are from Table 2 of Peeters et al. (2002).

1300 cm^{-1} (7.7 μm). In model II the lower wavelength component around 1347 cm^{-1} (7.42 μm) with shoulder at 1325 cm^{-1} (7.55 μm) dominates, while the higher wavelength sub-feature at 1285 cm^{-1} (7.78 μm) is less intense. Profiles similar to models I and II, with a stronger lower wavelength component, have been observed in UV-rich environments of HII regions and reflection nebulae and have been classified as A' profiles (Fig. 13 in Peeters et al. 2002). Medium-sized compact PAHs with 40–50 carbon atoms, as present in model II, are quite stable and may survive in strong UV environments providing good representation of PAHs populating such interstellar sources. Observations also indicate that sources dominated by the 7.6 μm sub-feature always exhibit a distinct 7.8 μm sub-feature (Peeters et al. 2002). Model II fulfills this observational norm well.

In model III with large PAHs, the 7.7 μm band is dominated by the higher wavelength sub-component at 1285 cm^{-1} (7.78 μm) with an apparent shoulder around 1315 cm^{-1} (7.60 μm). Unlike model II it is not distinctly resolved but appears as a shoulder to the main peak. Observations show that sources with a dominant 7.8 μm component do not always have a very clear and distinctive 7.6 μm component (Peeters et al. 2002; Bregman & Temi 2005). The profile of model III conforms to these observations of relatively benign astrophysical regions classified as B' profiles (Peeters et al. 2002).

For direct comparison and matching with observations, intensity ratios of the two components of the 7.7 μm complex and their wavenumber separation in the three models is presented in Table 1. Similar ratios from observations by Peeters et al. (2002) have also been provided. A good match in terms of intensity ratio is present with different observed sources. The profile observed in model I is similar to the classification A'. Model II shows a separation of almost 62 cm^{-1} between the two components of the composite 7.7 μm band with an intensity ratio of 1.06. The separation is a bit more than observed for A' profiles. The intensity ratio is also less than what is measured for NGC 2023 but is closer to that in IRAS 23133. Similar match has been shown to exist with the co-added spectra of medium sized pericondensed PAH cations (Pathak & Rastogi 2006). Model III shows a clear agreement with the observed B' profiles. The separation between the two components of the 7.7 μm band as well as the intensity ratio match well especially for NGC 7027.

The region of 6.2 μm feature, i.e. 1450 to 1650 cm^{-1} region of Fig. 3, is expanded in Fig. 5. There is no position match with the 6.2 μm (1610 cm^{-1}) AIB in any of the three models. The co-added spectra of small PAHs (model I) has this band centered on 1526 cm^{-1} (6.55 μm), which is far off the observed 6.2 μm band. As the PAH size increases, a blue shift, similar to available experimental data (Hudgins & Allamandola 1999b), is observed. The co-added spectra of medium-sized PAHs (model II) has this feature at 1537 cm^{-1} (6.51 μm) and only a small additional shift to 1564 cm^{-1} (6.39 μm) is present for large PAHs (model III). A few PAH cations e.g., $C_{28}H_{14}$, $C_{38}H_{16}$, and $C_{90}H_{24}$ (Pathak & Rastogi 2006, 2007) independently show intense features around 6.29 μm (1590 cm^{-1}) corresponding to the observed class C band (Peeters et al. 2002). These PAHs contribute to the small shoulder observed beyond 1590 cm^{-1} (6.29 μm).

Failure to explain the position of the 6.2 μm AIB with co-added model spectra of pure PAHs points towards other possibilities. Recent theoretical calculations of nitrogen substituted large PAH cations (PANHs) proposes to explain the variations in the peak position of the 6.2 μm interstellar emission feature (Hudgins & Allamandola 2003; Hudgins et al. 2005). Incorporating nitrogen inside the ring, i.e., replacing one or more carbon atoms results in a shift of the band from 6.4 μm to 6.2 μm. A similar blue shift is also reported for the iron – PAH coordination complex (Simon & Joblin 2007). Hydrogenated, dehydrogenated, and multiply-charged PAHs, PAH clusters, anions, and substituted PAHs (Bakes et al. 2001a; Halasinski et al. 2005; Malloci et al. 2005, 2007; Vuong & Foing 2000) also need careful attention and cannot be completely neglected. Either these or a combination of these with pure PAH ions may be responsible for the 6.2 μm emission feature.

3.2. C–H out-of-plane bend modes

The 11.2 μm (893 cm^{-1}) AIB represents solo out-of-plane wag modes in PAHs. The weak 12.7 μm (787 cm^{-1}) band and features at longer wavelengths represent trio and quartet hydrogen wag modes. ISO observations by Hony et al. (2001) conclude that the spectra of planetary nebulae and evolved carbon-rich stars, where PAHs are supposed to be synthesized and are still unprocessed, have a strong 11.2 μm feature, weak 12.7 μm band, and features at longer wavelengths. The situation is almost reversed in the case of UV-rich environments where the 12.7 μm band is as intense as the 11.2 μm band.

The spectra of small (model I) and medium-sized (model II) neutral PAHs (Fig. 6) have strong quartet hydrogen wag modes peaking around 750 cm^{-1}. Mixing of duo and trio hydrogen wags result in a broad peak around 815 cm^{-1} in small PAHs. For PAHs comprising 20 to 40 carbon atoms (model II), the intense solo wag mode near 900 cm^{-1} (11.11 μm) shows the best position and an intensity agreement with the observed 11.2 μm AIB. The spectrum of model III has this feature blue-shifted to around 915 cm^{-1} (10.93 μm). Model III also displays discrete, less intense features due to duo and trio hydrogen out-of-plane bend vibrations at 840 and 800 cm^{-1}, respectively.

Upon ionization the C–H out-of-plane bend modes in all the PAHs show significant shift in band positions but intensity variations are small (Fig. 6). Model I has intense peak at

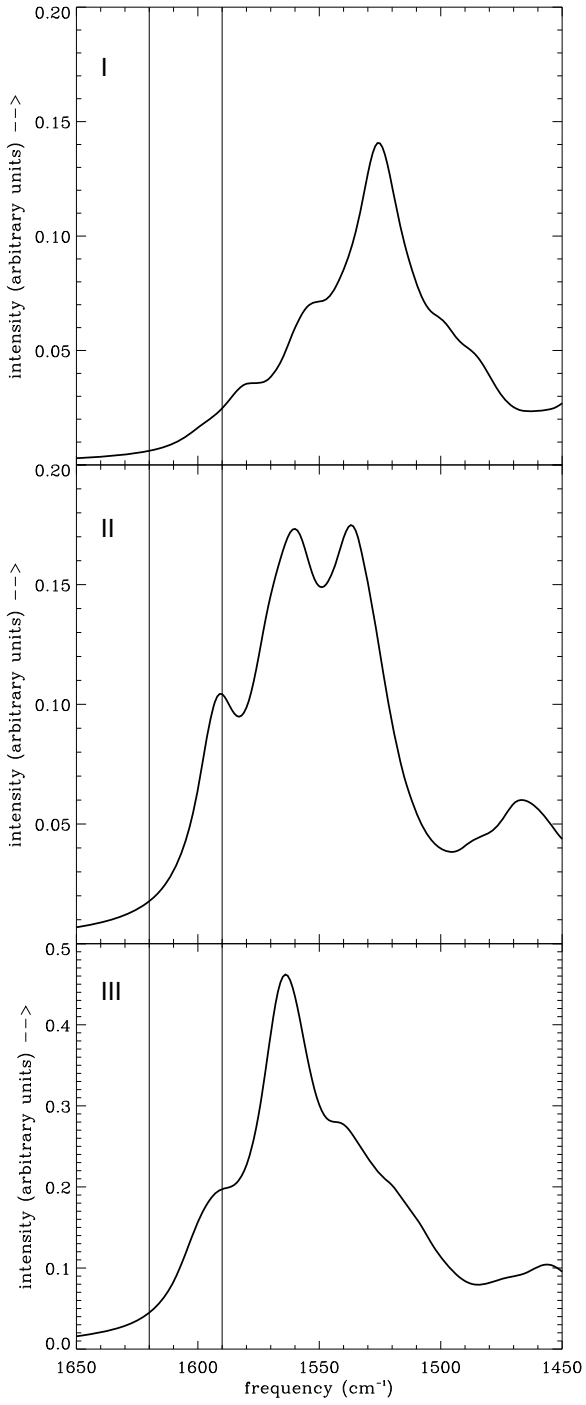

Fig. 5. Emission spectra of three cation models in the 1450 to 1650 cm^{-1} region. The observed 6.2 μm AIB lies within the two parallel lines.

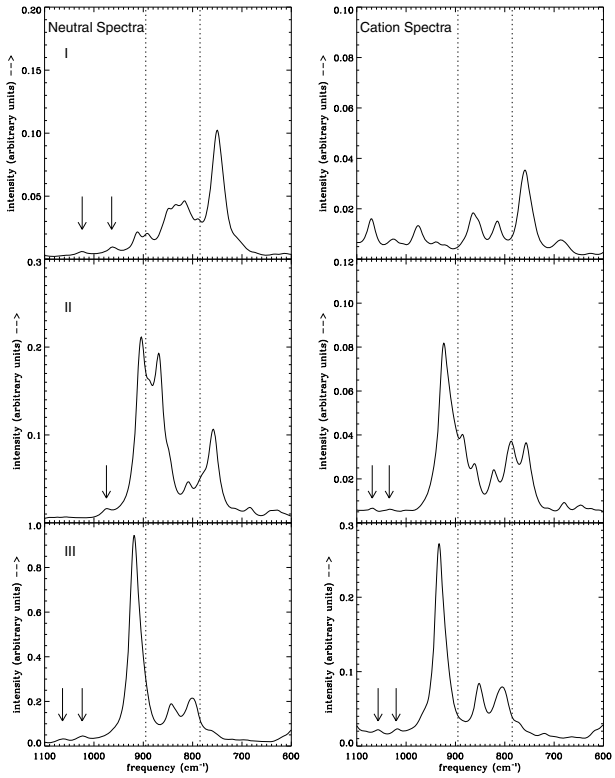

Fig. 6. Emission spectra of three models in the 600 to 1100 cm^{-1} region. Arrows point to blue outliers of 11.2 μm band. Dotted vertical lines represent central peak of 11.2 and 12.7 μm AIB.

Table 2. Intensity ratios[a] for the main PAH features.

Model	6.2/7.7 (PAH^+)	6.2/11.2 (PAH^+)	7.7/11.2 (PAH^+)	11.2/12.7 (Neutral PAH)
Model I	1.15	7.65	6.66	0.44
Model II	1.22	2.12	1.74	2.00
Model III	1.01	1.70	1.68	4.39

[a] Ratios are for emission models as in Figs. 2 and 3.

760 cm^{-1} (13.16 μm) and a less intense feature at 864 cm^{-1} (11.57 μm). These features in model I correlate with observations of weak bands present on the long wavelength side of the 11.2 μm band (Witteborn et al. 1989). The co-added emission spectra of medium-sized (model II) PAH cations has an intense feature at 920 cm^{-1} and significant peaks at 755 and 785 cm^{-1}. Large PAH cations (model III) have prominent solo hydrogen (C−H) out-of-plane bend modes producing an intense peak at 933 cm^{-1} and weak features between 800 and 850 cm^{-1}. The shifts in band positions of hydrogen out-of-plane modes with ionization and increasing PAH size are apparent in the three models.

Sloan et al. (1999) observed complex, less intense structures on the short wavelength side of the principal 11.2 μm AIB. They refer to them as "blue outliers". These blue outliers were more noticeable near the central exciting object. The 11.2 μm feature adopts a smoother profile in observations away from the central source with weak or no blue outliers. These observations correlate with our models (Fig. 6). The existence of stable compact medium-sized PAHs or cations in the vicinity of the central source is one possibility. This also correlates with the observation that UV-rich environments where 6.2 and 7.7 μm show the *A* type profile and also have *A* type 11.2 μm band (Van Diedenhoven et al. 2004).

3.3. Intensity ratios

The intensity of the AIBs may not be directly correlated with spectral models based on theoretical or experimental measurements, but the ratios of different features prove to be highly useful. Systematic variations associated with intensity ratios for

different modes may be used to constrain PAH size, structure, and ionization state in the ISM. In neutral PAHs, where the spectra is dominated by C−H stretch and wag modes with weak C−C stretch mode intensities, the 6.2 and 7.7 μm to 11.2 μm band ratio is small; but for cations, there is a tremendous increase in the value, which is an indicator of the ionization state of PAHs. The emission model intensity ratios of a few features are presented in Table 2. Since the models fail to reproduce the 6.2 μm feature, the presented ratios are not directly relevant to observations but do point towards a trend.

For cations, the value for the 6.2 to 7.7 μm band ratio is lowest for large PAHs. The ratio of 11.2 to 12.7 μm PAH bands for neutral PAHs sheds light on the shape (peripheral structure) of PAHs (Hudgins & Allamandola 1999a; Hony et al. 2001). As the PAH size increases, the ratio appears to increase steadily. Since, small PAHs inevitably have more corners, leading to more duo and trio hydrogens, the intensity of their wag is strong. The compact and stable large PAHs considered in the models have straight edges resulting in an increased number of solo hydrogens, and the spectra have an intense 11.2 μm band.

3.4. PAH formation and processing

The correlation of observations with model spectra from collective emission of PAHs presented in this report leads to understanding the formation and processing of PAHs in the ISM. The correlation of 7.7 μm B' profile with model III suggests formation of large PAHs (having around 100 carbon atoms) in outflows of late-type carbon-rich stars. Since, ionization energy for large PAHs is weaker, they are more likely to be cations. The spectra of these large PAH cations dominate benign regions of the ISM. Observations of the 6.3 μm (1585 cm^{-1}) AIB (C class; Peeters et al. 2002) in these regions suggests that the PAHs initially formed are pure and unsubstituted. The processing of these large systems starts as soon as they are formed. Ruled by the ISM conditions, equilibrium is established between formation and destruction. A likely scenario is that, in harsh ISM conditions, breaking and reduction of large structures along with multiple ionization of medium-sized PAHs dominates. Observation of A' profiles in UV-rich environments of ISM suggests the abundance of compact medium-sized PAH cations. This is also confirmed by the observation of a strong 12.7 μm band in UV-rich environments. Formation of multiply charged PAHs, substituted PAHs (PANHs), PAH complexes, and clusters is suggested by the observation of a 6.2 μm A class profile in harsh strong UV flux environments (Peeters et al. 2002).

Taking the cue from these models, more specific modeling for particular observations can be made by varying the concentrations of the individual PAHs. These can provide better understanding of the chemistry of the region. A combination of PAHs from models I and II with different concentrations is taken to compare with the observed 7.7 μm feature of reflection nebula NGC 2023. The most suitable combination obtained has Perylene (14%), Triphenylene (11%), Benzo-pyrene (9%), Ovalene (25%), Bisanthene (9%), $C_{30}H_{14}$ (17%), $C_{38}H_{16}$(15%) and is shown in Fig. 7a. The lower wavelength component dominates the 7.7 μm band, while the higher wavelength sub-feature is slightly less intense. These have been classified as A' profiles (Peeters et al. 2002) as observed in UV-rich environments of HII regions, reflection nebulae, and other star-forming regions. Starburst galaxies, where there is copious star formation activity, also have similar profile (e.g. average spectra of 11 Starbursts Fig. 1 Lutz et al. 1998). The 7.7 μm band in galaxies is useful in the study of AGN–Starburst connection (Schweitzer et al. 2006; Tran et al. 2001; Lutz et al. 1998).

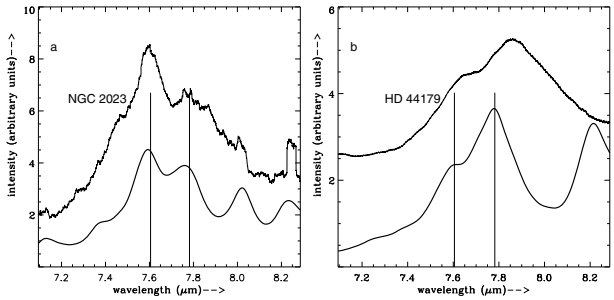

Fig. 7. PAH cations emission model in the 1200 to 1400 cm^{-1} region compared with observed spectra **a)** PAHs with less than 40 C atoms in varying proportions (see text); **b)** more than 40 C atoms (model III). The 7.7 μm band lies within the two vertical lines.

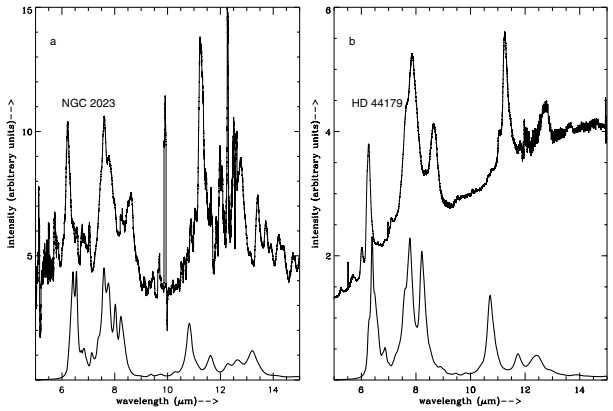

Fig. 8. Same as Fig. 7 in the range 5–15 μm. **a)** PAHs with less than 40 C atoms in varying proportions (see text); **b)** more than 40 C atoms (model III).

Figure 7b compares the 7.7 μm feature of model III with post-AGB star HD 44179, which is classified as B' profile (Peeters et al. 2002) of relatively benign astrophysical regions where PAHs are supposed to be synthesized. A slight shift in the band position and an additional feature near 1215 cm^{-1} (8.2 μm) mark the difference in agreement with observations.

It is interesting to compare the models with observation over the whole range from 5–15 μm, as shown in Fig. 8. Though there is gross similarity, in both cases it is seen that prominent features apart from the 7.7 μm band are either shifted or have an intensity mismatch. The 6.2 μm band lies at a higher wavelength, while the 11.2 μm band is blue-shifted in the model spectra. Considering PAH population in ISM to be even partially similar to the present models, observations should show the strong features of the models e.g. around 6.5 and 10.8 μm.

4. Conclusions

AIBs are ubiquitous in diverse astrophysical sources with their origin commonly ascribed to interstellar PAHs. Recent space-based observations have enabled high-quality infrared data, which has introduced variations in profiles of the observed mid-IR spectra. These variations correlate with the object type and are indicative of PAH populations existing in different sources. To gain insight into the profile variations of PAH bands and to interpret them better, three distinct models using PAHs of different size groups are presented. Correlation of these models with

observations throws light on the formation and processing of PAHs in different astrophysical environments.

The models show good profile matches with observations for the 7.7 μm band. This feature is not a single peak but a combination of two sub-components at 7.6 and 7.8 μm that are also distinct in the presented models. The 7.6 μm sub-feature is found to dominate in the spectra of small to medium-sized PAH cations matching with the observations of UV-rich interstellar environments (Fig. 7a). The 7.8 μm component is more intense in the spectra of large PAH cations correlating with the observations of benign astrophysical regions (Fig. 7b). This clearly indicates the formation of large PAHs in the outflows of carbon-rich stars that transform to medium-sized ones upon processing.

The models also correlate well with the observations of the C−H out-of-plane bend modes and the weak outliers on the blue side of the intense 11.2 μm band. The variation in the observed intensity of 12.7 and 11.2 μm bands points towards large PAHs in planetary nebula and medium and small PAHs in UV-rich environments of HII regions and reflection nebula.

Varying concentrations of the individual PAHs and considering the strength of exciting radiation may allow modeling of specific astrophysical objects. But the feature corresponding to 6.2 μm AIB is not correlated with the present set of PAHs. Also, strong features of the models, around 6.5, 8.2, and 10.8 μm, should show up in observations if the PAH population in ISM is similar to those considered here. The models presented do provide pointers to possible PAH populations in different regions, yet the same group of PAHs should provide a match for all the AIBs for a complete and realistic model.

Failure to explain the complete profile of AIBs may be due to the incompleteness of the sample. A bigger sample of PAHs that includes substituted PAHs, PAH coordination complexes, hydrogenated and de-hydrogenated PAHs, and different charge and ionization states of all these may be required. Since laboratory data for most of these systems may be difficult to obtain, quantum chemical approach is most suitable, which needs to be refined by using larger basis sets. A better modeling approach should incorporate anharmonicity and hot band shifts. Some work has been done in this direction (Joblin et al. 1995; Pech et al. 2002; Mulas et al. 2006a,b; Cané et al. 2007), but exact identification of individual PAHs based on these is still difficult.

Acknowledgements. The authors are thankful to Dr. G. Mulas, the referee, for insightful suggestions and improvement in the paper's content. The use of High Performance Computing and the library facilities at Inter University Center for Astronomy and Astrophysics, Pune, is acknowledged.

References

Allain, T., Leach, S., & Sedlmayr, F. 1996a, A&A, 305, 602
Allain, T., Leach, S., & Sedlmayr, F. 1996b, A&A, 305, 616
Allamandola, L. J., Tielens, A. G. G. M., & Barker, J. R. 1985, ApJ, 290, L25
Allamandola, L. J., Tielens, A. G. G. M., & Barker, J. R. 1989, ApJS, 71, 733
Allamandola, L. J., Hudgins, D. M., & Sandford, S. A. 1999, ApJ, 511, L115
Bakes, E. L. O., Tielens, A. G. G. M., & Bauschlicher, C. W. 2001a, ApJ, 556, 501
Bakes, E. L. O., Tielens, A. G. G. M., Bauschlicher, C. W., Hudgins, D. M., & Allamandola, L. J. 2001b, ApJ, 560, 261
Bauschlicher, C. W. 2002, ApJ, 564, 782
Bauschlicher, C. W., & Bakes, E. L. O. 2000, Chem. Phys., 262, 285
Bregman, J. D., & Temi, P. 2005, ApJ, 621, 831
Bregman, J. D., Allamandola, L. J., Tielens, A. G. G. M., Geballe, T. R., & Witteborn, F. C. 1989, ApJ, 344, 791
Cané, E., Miani, A., & Trombetti, A. 2007, J. Phys. Chem. A, 111, 8218
Cohen, M., Tielens, A. G. G. M., Bregman, J. D., et al. 1989, ApJ, 341, 246
Cook, D. J., & Saykally, R. J. 1998, ApJ, 493, 793
Cook, D. J., Schlemmer, S., Balucani, N., et al. 1996, Nature, 380, 227
DeVito, B., & Hayward, T. L. 1998, ApJ, 504, 43
Geballe, T. R., Tielens, A. G. G. M., Allamandola, L. J., Moorhouse, A., & Brand, P. W. J. L. 1989, ApJ, 341, 278
Gillett, F. C., Forrest, W. J., & Merrill, K. M. 1973, ApJ, 183, 87
Halasinski, T. M., Salama, F., & Allamandola, L. J. 2005, ApJ, 626, 555
Hony, S., van Kerckhoven, C., Peeters, E., et al. 2001, A&A, 370, 1030
Hudgins, D. M., & Allamandola, L. J. 1995, J. Phys. Chem., 99, 3033
Hudgins, D. M., & Sandford, S. A. 1998, J. Phys. Chem. A 102, 394
Hudgins, D. M., & Allamandola, L. J. 1999a, ApJ, 516, L41
Hudgins, D. M., & Allamandola, L. J. 1999b, ApJ, 513, L69
Hudgins, D. M., & Allamandola, L. J. 2003, Astrophysics of Dust (San Francisco: ASP), ed. A. N. Witt, G. C., Clayton, & B. T. Draine, ASP Conf. Ser., 309, 665
Hudgins, D. M., Sandford, S. A., & Allamandola, L. J. 1994, J. Phys. Chem., 98, 4243
Hudgins, D. M., Bauschlicher, C. W., & Allamandola, L. J. 2001, Spectrochim. Acta A, 57, 907
Hudgins, D. M., Bauschlicher, C. W., & Allamandola, L. J. 2005, ApJ, 632, 316
ISO Results 1996, A&A, 315, L26
Joblin, C., Boissel, P., Léger, A., d'Hendecourt, L., & Defourneau, D. 1995, A&A, 299, 835
Joblin, C., Toublanc, D., Boissel, P., & Tielens, A. G. G. M. 2002, Mol. Phys. 100, 3595
Kim, H. S., & Saykally, R. J. 2002, Ap&SS, 143, 455
Kim, H. S., Wagner, D. R., & Saykally, R. J. 2001, Phys. Rev. Lett., 86, 5691
Langhoff, S. R. 1996, J. Phys. Chem., 100, 2819
Léger, A., & Puget, J. L. 1984, A&A, 137, L5
Léger, A., d'Hendecourt, L., & Defourneau, D. 1989, A&A, 216, 148
LePage, V., Snow, T. P., & Bierbaum, V. M. 2003, ApJ, 584, 316
Li, A., & Draine, B. T. 2002, ApJ, 572, L232
Lutz, D., Spoon, H. W. W., Rigopoulou, D., Moorwood, A. F. M., & Genzel, R. 1998, ApJ, 505, L103
Malloci, G., Mulas, G., Cappellini, G., Fiorentini, V., & Porceddu, I. 2005, A&A, 432, 585
Malloci, G., Joblin, C., & Mulas, G. 2007, Chem. Phys., 332, 353
Mattioda, A. L., Allamandola, L. J., & Hudgins, D. M. 2005a, ApJ, 629, 1183
Mattioda, A. L., Allamandola, L. J., & Hudgins, D. M., 2005b, ApJ, 629, 1188
Mulas, G., Malocci, G., & Benvenuti, P. 2003, A&A, 410, 639
Mulas, G., Malocci, G., Joblin, C., & Toublanc, D. 2006a, A&A, 446, 537
Mulas, G., Malocci, G., Joblin, C., & Toublanc, D. 2006b, A&A, 460, 93
Pathak, A. 2006, Ph.D. Thesis, D.D.U. Gorakhpur University, Gorakhpur, India
Pathak, A., & Rastogi, S. 2005, Chem. Phys., 313, 133
Pathak, A., & Rastogi, S. 2006, Chem. Phys., 326, 315
Pathak, A., & Rastogi, S. 2007, Spectrochim. Acta A, 67, 898
Pech, C., Joblin, C., & Boissel, P. 2002, A&A, 388, 639
Peeters, E., Hony, S., van Kerckhoven, C., et al. 2002, A&A, 390, 1089
Peeters, E., Allamandola, L. J., Hudgins, D. M., Hony, S., & Tielens, A. G. G. M. 2004a, Astrophysics of Dust (San Francisco: ASP), ed. A. N. Witt, G. C. Clayton, & B. T. Draine, ASP Conf. Ser., 309, 141
Peeters, E., Mattioda, A. L., Hudgins, D. M., & Allamandola, L. J. 2004b, ApJ, 617, L65
Puget, J. L., & Léger, A. 1989, ARA&A, 27, 161
Schmidt, M. W., Baldridge, K. K., Boatz, J. A., et al. 1993, J. Comput. Chem., 14, 1347
Schutte, W. A., Tielens, A. G. G. M., & Allamandola, L. J. 1993, ApJ, 415, 397
Schweitzer, M., Lutz, D., Sturm, E., et al. 2006, ApJ, 649, 79
Simon, A., & Joblin, C. 2007, J. Phys. Chem. A, 111, 9745
Sloan, G. C., Hayward, T. L., Allamandola, L. J., et al. 1999, ApJ, 513, L65
Sloan, G.C., Keller, L.D., Forrest, W. J., et al. 2005, ApJ, 632, 956
Smith, T. L., Clayton, G. C., & Valencic, L. 2004, AJ, 128, 357
Spitzer results, 2004, ApJS, 154
Szczepanski, J., & Vala, M. 1993, Nature, 363, 699
Tran, Q. D., Lutz, D., Genzel, R., et al. 2001, ApJ, 552, 527
Van Diedenhoven, B., Peeters, E., Van Kerckhoven, C., et al. 2004, ApJ, 611, 928
Vijh, U. P., Witt, A. N., & Gordon, K. D. 2005, ApJ, 633, 262
Vuong, M. H., & Foing, B. H. 2000, A&A, 363, L5
Werner, M. W., Uchida, K. L., Sellgren, K., et al. 2004, ApJS, 154, 309
Witt, A. N., Gordon, K. D., Vijh, U. P., et al. 2006, ApJ, 636, 303
Witteborn, F. C., Sandford, S. A., Bregman, J. D., et al. 1989, ApJ, 341, 270